11-27-2018

Structural, Magnetic, and Mössbauer Studies of Transition Metal-Doped Gd2Fe16Ga0.5TM0.5 Intermetallic Compounds (TM = Cr, Mn, Co, Ni, Cu, and Zn)

Jiba Dahal
Georgia Southern University, jdahal@georgiasouthern.edu

K. S. Syed Ali
Harmony Science Academy

S. R. Mishra
University of Memphis

J. Alam
University of Memphis

magnetochemistry

MDPI

Article

Structural, Magnetic, and Mössbauer Studies of Transition Metal-Doped $Gd_2Fe_{16}Ga_{0.5}TM_{0.5}$ Intermetallic Compounds (TM = Cr, Mn, Co, Ni, Cu, and Zn)

J. N. Dahal [1,2,*], K. S. Syed Ali [3], S. R. Mishra [2] and J. Alam [2]

1 Department of Physics and Astronomy, Georgia Southern University, Savannah, GA 31419, USA
2 Department of Physics and Materials Science, The University of Memphis, Memphis, TN 38152, USA; srmishra@memphis.edu (S.R.M.)
3 Department of Science, Harmony Science Academy, 12005 Forestgate Dr., Dallas, TX 75243, USA; kssyedali@gmail.com
* Correspondence: jdahal@georgiasouthern.edu; Tel.: +1-(912)-344-2842

Received: 9 September 2018; Accepted: 19 November 2018; Published: 27 November 2018

Abstract: The effect of transition metal substitution for Fe and the structural and magnetic properties of $Gd_2Fe_{16}Ga_{0.5}TM_{0.5}$ (TM = Cr, Mn, Co, Ni, Cu, and Zn) compounds were investigated in this study. Rietveld analysis of X-ray data indicates that all the samples crystallize in the hexagonal Th_2Ni_{17} structure. The lattice parameters *a*, *c*, and the unit cell volume show TM ionic radii dependence. Both Ga and TM atoms show preferred site occupancy for 12*j* and 12*k* sites. The saturation magnetization at room temperature was observed for Co, Ni, and Cu of 69, 73, and 77 emu/g, respectively, while a minimum value was observed for Zn (62 emu/g) doping in $Gd_2Fe_{16}Ga_{0.5}TM_{0.5}$. The highest Curie temperature of 590 K was observed for Cu doping which is 15 and 5% higher than Gd_2Fe_{17} and $Gd_2Fe_{16}Ga$ compounds, respectively. The hyperfine parameters viz. hyperfine field and isomer shift show systematic dependence on the TM atomic number. The observed magnetic and Curie temperature behavior in $Gd_2Fe_{16}Ga_{0.5}TM_{0.5}$ is explained on the basis of Fe(3d)-TM(3d) hybridization. The superior Curie temperature and magnetization value of Co-, Ni-, and Cu-doped $Gd_2Fe_{16}Ga_{0.5}TM_{0.5}$ compounds as compared to pure Gd_2Fe_{17} or $Gd_2Fe_{16}Ga$ makes $Gd_2Fe_{16}Ga_{0.5}TM_{0.5}$ a potential candidate for high-temperature industrial magnet applications.

Keywords: permanent magnetic materials; 2:17 intermetallic; Mössbauer spectroscopy; Curie temperature; X-ray diffraction; Rietveld analysis

1. Introduction

The rare-earth intermetallic compounds R_2Fe_{17} have energy product $(BH)_{max}$ and *Hc* to be about 26 MGOe and 15 kOe, respectively [1]. Beside these properties, they exhibit low Curie temperature (*Tc*). For example, 473 K for Gd_2Fe_{17} and 300 K for Dy_2Fe_{17} along with low magnetic anisotropies [2]. Various strategies have been employed addressing issues related to improving magnetic anisotropy, magnetization, and Curie temperature of R_2Fe_{17} compounds. Metalloids such as C, N, and H atoms are added to improve the magnetic anisotropy and Curie temperature [3–6]. However, high-temperature processing of these interstitially modified compounds is difficult. Subsequently, the addition of non-magnetic atoms such as Al, Ga, and Si for iron in the $R_2Fe_{17-x}M_x$ compound was investigated and showed Curie temperature enhancement at high non-magnetic atom content. Among Al, Si, and Ga, Ga substituted compounds show high *Tc*, e.g., for $Sm_2Fe_{16}Ga$, *Tc* was ~485 K [7]; for $Dy_2Fe_{16}Ga$, *Tc*

was ~462 K [8]. However, this improvement in *Tc* is overshadowed by a concomitant deterioration in saturation magnetization as iron atoms are being replaced by non-magnetic atoms.

The Curie temperatures T_c in the R_2Fe_{17} compounds is explained on the basis of exchange interaction strength between Fe–Fe pairs [9]. This is based on the assumption that the exchange interactions favor ferromagnetic ($r > r_c$) or antiferromagnetic ($r < r_c$) properties, where r_c ~2.5 Å. Hence, *Tc* is assumed dependent on the competition between ferromagnetic and antiferromagnetic exchange interactions between neighboring pairs of Fe–Fe ions located at various crystallographic positions. This means that *Tc* enhancement can be achieved via lattice unit cell expansion, except in Si-substituted $RE_2Fe_{17-x}Si_x$, favoring ferromagnetic exchange interaction between Fe–Fe pairs. Usually, such lattice expansion is possible either via substituting for Fe ions by ions with the larger ionic radii [10,11] or via insertion of interstitial atoms in the unit cell [12,13]. It was observed that there are two ingredients influencing T_C value: local magnetic moment values and exchange interaction values [14].

Among R_2Fe_{17} intermetallic, Gd_2Fe_{17} is of special interest, as it has the highest Curie temperature, T_C. Among the doped $R_2Fe_{17-x}M_x$ (M = Al, Si, Ga), Ga-doped compounds display higher *Tc* [15]. In this regard, the present work investigates the effect of doping transition metal (TM) atoms in Ga-doped $Gd_2Fe_{16}Ga_{0.5}TM_{0.5}$ compounds and compares the results with Gd_2Fe_{17}. It is expected that the doping of TM atoms with ionic radii greater than Fe will bring unit cell volume expansion and hence improve Fe–Fe exchange interaction enough to couple Fe–Fe moments ferromagnetically, thus improving the Curie temperature of the compound. Furthermore, there also lies the possibility of improving magnetic moment of Fe via Fe–TM 3d band hybridization, which can either bring band narrowing or increase exchange splitting by moving the 3d↑ states below the Fermi level or allow charge transfer out of the 3d band, provided that the spin-down density of states exceed the spin-up density [16].

This study discusses the change in the structural and magnetic properties in R_2Fe_{17} compounds when Fe is substituted in $R_2Fe_{16}Ga_{0.5}TM_{0.5}$ compounds with transition metal TM = Cr, Mn, Co, Ni, Cu, and Zn. The main aim of the study is to bring structural and band-related changes to R_2Fe_{17} compounds so as to improve *Tc* without affecting the saturation magnetization.

2. Experimental Section

The raw materials of Gd, Fe, Ga, and TM (TM = Cr, Mn, Co, Ni, Cu, and Zn) with 99.9% purity were purchased from Sigma Aldrich, USA. The parent alloys $Gd_2Fe_{16}Ga_{0.5}TM_{0.5}$ were prepared by arc melting the stoichiometric amount of the aforementioned elements under a high purity argon atmosphere. The ingots were melted several times to ensure the high degree of homogeneity.

X-ray diffraction (XRD) experiment was carried out with Cu K_α (λ ~1.5406 Å) radiation using a Bruker (D8 Advance) diffractometer. The powder X-ray data sets were collected in the 2θ range from 20 to 75° with a step size of 0.042° and a collection time of 2 s/step. The XRD analysis was performed by the well-known structural refinement Rietveld method [17] using the JANA2006 [18] software package to fit the experimental and calculated diffraction patterns. The initial crystal structure parameters were used as given by Liao et al. [19]. In the hexagonal setting, Gd was fixed at the 2*b* and 2*d* site (0, 0, 0.25) and (0.333, 0.667, 0.75), Fe is fixed at 4*f*, 6*g*, 12*j*, and 12*k* (0.333, 0.667, 0.105), (0.5, 0, 0), (0.333, 0.969, 0.25), and (0.167, 0.333, 0.985). The profile was constructed using a pseudo-Voigt function. Profile asymmetry was introduced by employing the multi-term Simpson rule integration devised by Howard [20]. A surface roughness correction was also applied using the Pitschke, Hermann, and Matter [21] model. In this technique, structural parameters, lattice parameters, peak shift, background profile shape, and preferred orientation parameters were used to minimize the difference between a calculated profile and the observed data.

Magnetic properties of the powder sample were investigated at room temperature (RT) using a vibrating sample magnetometer (VSM) in the maximum field of 1.2 T. To minimize the effect of the demagnetizing field, the samples were compacted at 3000 psi, cut into rectangular parallelepiped with the length-to-width ratio greater than 3, and embedded in epoxy. A modified thermogravimetric

analyzer (DuPont 910) equipped with a permanent magnet was used to determine the Curie temperature of composite samples. In this procedure, magnetic material is placed inside an empty, tared, TGA pan located near a strong magnet. The material is then heated. At the Curie temperature, *Tc*, the magnetic properties disappear (i.e., the material goes from ferromagnetic to paramagnetic), and the reduced attraction for the magnet results in a sharp apparent weight loss or gain (depending on the TGA design).

The Mössbauer spectra of the samples were obtained at RT using a 25 mCi ^{57}Co source in a Rh foil mounted on a constant acceleration drive system (SEE Co., Minneapolis, MN, USA) in transmission geometry. The velocity scale of the Mössbauer spectrometer was calibrated by measuring the hyperfine field of α-Fe foil, at room temperature. The Mössbauer spectra were analyzed using WMoss software from SEE Co. They were fitted using a standard nonlinear least squares minimization routine with sub-spectra intensities constrained to match crystallographic probabilities.

3. Results and Discussion

The raw powder profile for $Gd_2Fe_{16}Ga_{0.5}TM_{0.5}$ systems is presented in Figure 1a. The inset in Figure 1a, the enlarged 2θ view between 41.5 and 43.3°, shows that there is a shift in 2θ towards the lower angle, which indicates the expansion of the unit cell with the substitution of increasing atomic number of TM in the compound. This observation is in accordance with the increasing size of the substitution atom whose metallic radii increases from TM = Cr to Zn (Table 1). The refined Rietveld profiles are presented in Figure 1b for $Gd_2Fe_{16}Ga_{0.5}TM_{0.5}$ systems. In Table 1, the R_{obs} values are calculated from the observed and calculated structure factors. Since it is a mixed system, the R_{obs} possibly adds errors (less than 5%) in the structure factor. These small errors reflect on the low angle, and the intensity counts range is between 25 and 100, which is minimal. This error may be because of multiple factors such as background errors, the preferred orientation, multiplicity factors, and instrumental errors. Moreover, these errors are minimal when compared to the high angle reflection 2θ range of 35–45°. The refined structural parameters viz. lattice parameters *a*, *c*, the *c/a* ratio, the unit cell volume, and the reliability indices are given in Table 1. From the Rietveld analysis, the refined profile indicates that $Gd_2Fe_{16}Ga_{0.5}TM_{0.5}$ compounds crystallize in the hexagonal Th_2Ni_{17} structure with the $P6_3/mmc$ symmetry group. Figure 2 show the lattice parameters as a function of the TM atomic number in $Gd_2Fe_{16}Ga_{0.5}TM_{0.5}$. It can be observed in Figure 2 that the variation in lattice parameter, *a*, is more pronounced than that in *c* in the doped compounds. This is also evident from the variation in the *c/a* ratio (Table 1), which indicates the anisotropic expansion of unit cell volume with TM atom doping. The doping of Cr up to Co brings lattice contraction while Ni, Cu, and Zn brings about lattice expansion. The observed trend in lattice parameter closely follows TM metallic radii (Figure 2).

Table 1. Structural parameters derived from Rietveld refinement of powder XRD data of Gd_2Fe_{17} and $Gd_2Fe16Ga_{0.5}TM_{0.5}$ (TM = Cr, Mn, Co, Ni, Cu, Zn, and Ga).

Parameter	Cr	Mn	Gd_2Fe_{17} Fe	Co	Ni	Cu	Zn	$Gd_2Fe_{16}Ga$ Ga
Metallic radii (pm)	127	126	129	125	125	128	136	140
a (Å)	8.5149(43)	8.5267(42)	8.4791(21)	8.4911(81)	8.4812(24)	8.4997(32)	8.5435(52)	8.5555(61)
c (Å)	8.3320(32)	8.3521(22)	8.3326(6)	8.3421(8)	8.3338(32)	8.3451(16)	8.3641(62)	8.3682(33)
c/a	0.9785	0.9795	0.9827	0.9824	0.9826	0.9818	0.9790	0.9781
Cell Volume (Å^3)	526.97	527.32	522.2634	525.15	523.60	526.06	528.21	528.5749
R_{obs} (%)	5.67	4.44	2.48	4.53	3.21	3.99	2.31	6.43
wR_{obs} (%)	4.32	5.21	3.55	5.31	4.21	4.87	3.65	7.12
R_P (%)	6.22	7.87	9.12	8.11	7.32	7.22	5.32	10.55
wR_P (%)	7.87	8.86	10.54	9.32	8.32	10.11	7.78	12.54

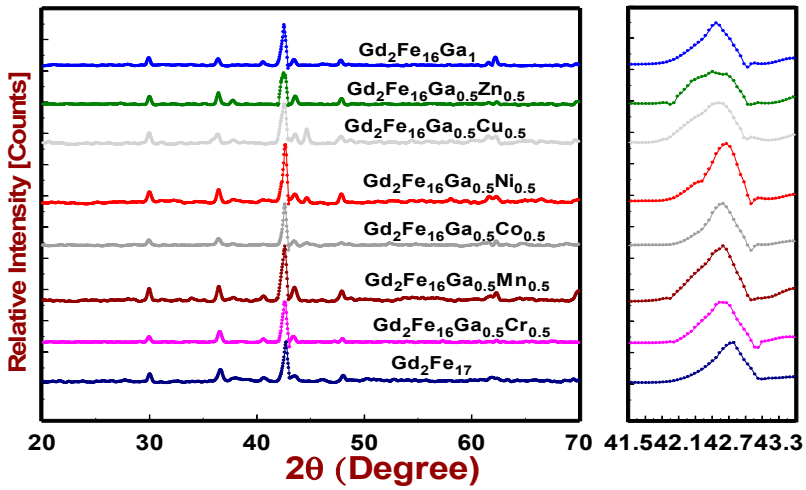

(**a**)

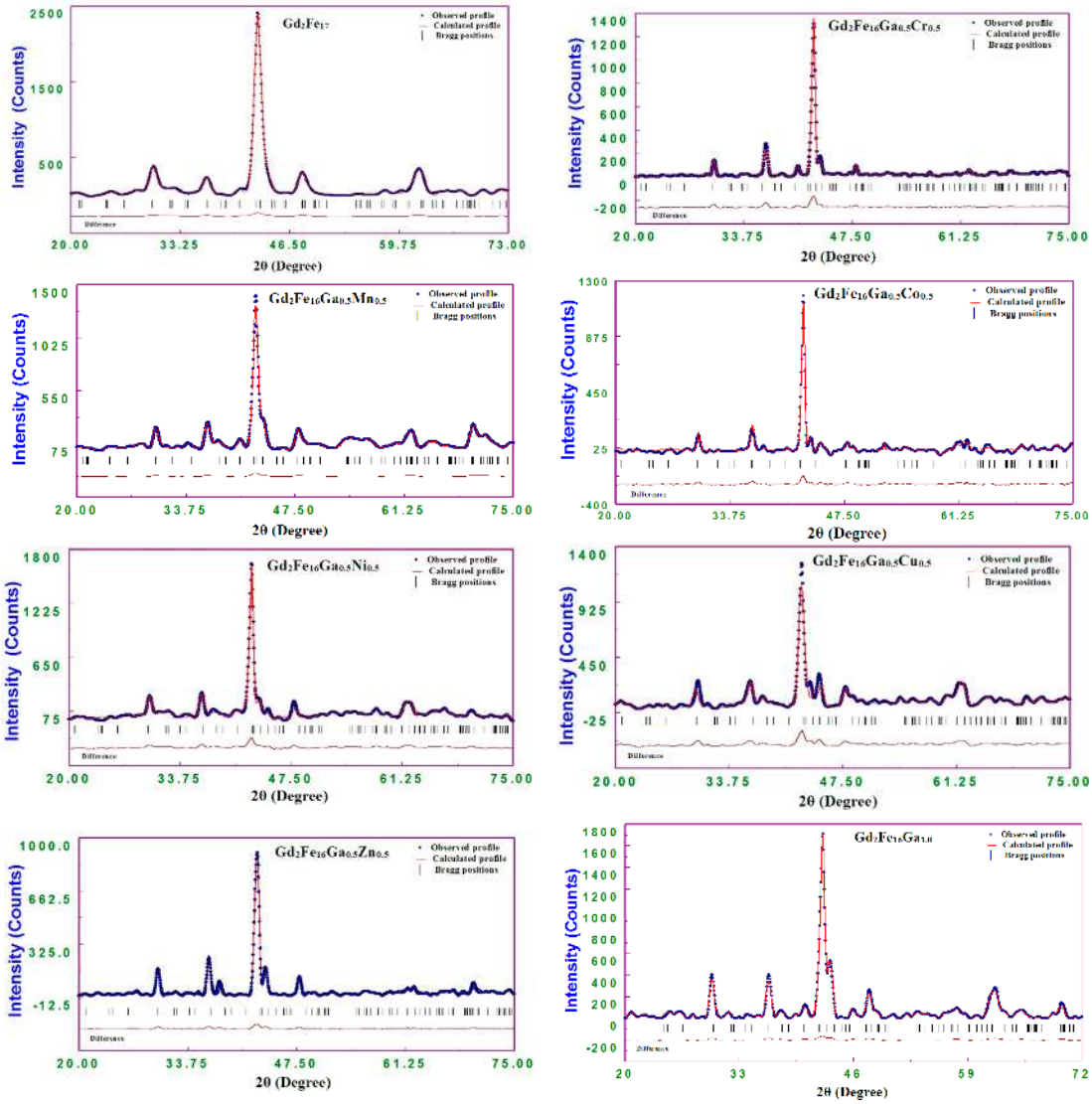

(**b**)

Figure 1. (**a**) XRD powder profile for Gd_2Fe_{17} and $Gd_2Fe_{16}Ga_{0.5}TM_{0.5}$ (TM = Cr, Mn, Co, Ni, Cu, Zn, and Ga). (**b**) Rietveld refined XRD data of Gd_2Fe_{17} and $Gd_2Fe_{16}Ga_{0.5}TM_{0.5}$ (TM = Cr, Mn, Co, Ni, Cu, Zn, and Ga).

The atomic site occupancy for Gd, Fe, Ga, and TM atoms derived from Rietveld refinement are listed in Table 2. The site notations are given for rhombohedral structure with corresponding hexagonal notation viz. 6*c*(4*f*), 9*d*(6*g*), 18*f*(12*j*), and 18*h*(12*k*). The crystallographic site preference exhibited by TM in $Gd_2Fe_{16}Ga_{0.5}TM_{0.5}$ is listed in Table 2. It is evident from Table 2 that Ga prefers 12*j* and 12*k* sites, and TM avoids 4*f* sites and prefers to remain closer to Ga at 12*j* and 12*k* sites. The TM atoms display occupancy preference with the order 12*j*~12*k* > 6*g* > 4*f*. Thus, the 6*c*(4*f*) dumbbell site is the least affected site by the TM substitution. Results of site occupancy are in close conformity with the previous Neutron diffraction [22,23] and ^{57}Fe Mössbauer studies [24–26] on $R_2Fe_{17-x}Ga_x$ where Ga atoms preferentially occupy mainly the 18*h*(12*k*) site in the Th_2Zn_{17} structure for $x < 4$. The number of Fe and R nearest neighbors (NNs) for Fe atoms at various crystallographic sites in R_2Fe_{17} compounds is as follows; at the Fe 6*c* site (dumbbell site), there are 13 Fe NNs and 1 R NNs; at the Fe 9*d* site, there are 10 Fe NNs and 2 R NNs; at Fe 18*f*, there are 10 Fe NNs and 2 R NNs; at the Fe 18*h* site there are 9 Fe NNs and 3 R NNs. In addition, the Wigner–Seitz cell volume follows 6*c*(4*f*) > 18*h*(12*k*) > 18*f*(12*j*) > 9*d*(6*g*). This shows that Ga and TM atoms for 12*j* and 12*k* sites suggest that the Ga affinity for R atoms surpasses the Wigner–Seitz site volume [15].

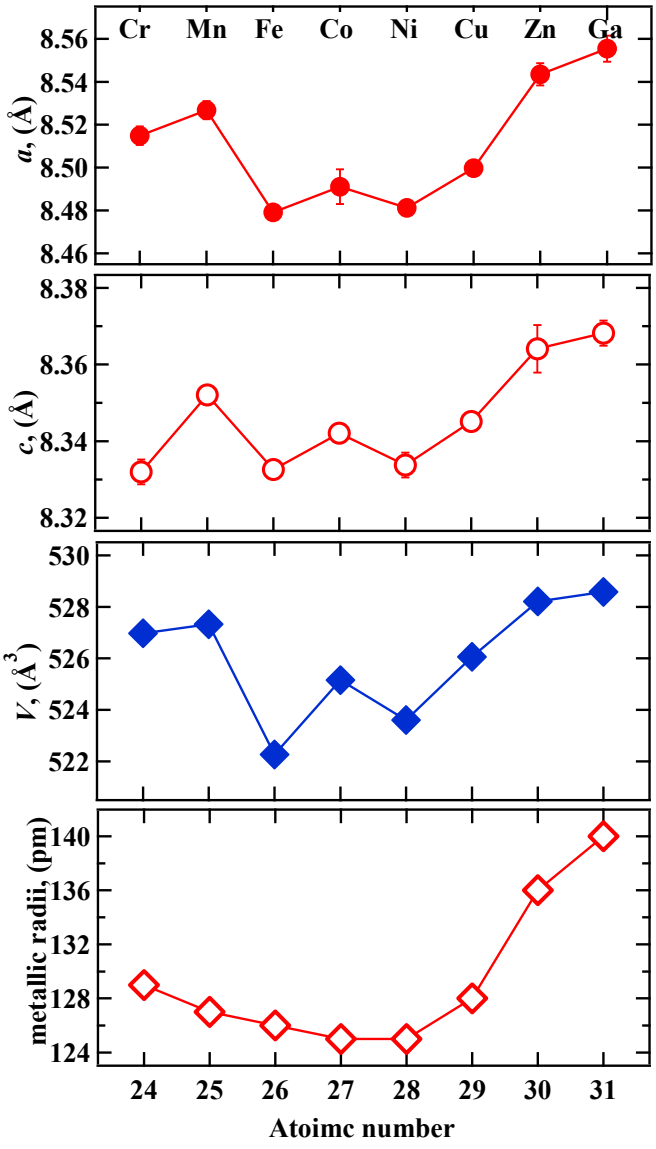

Figure 2. Lattice parameters obtained via Rietveld refinement, and metallic radii of $Gd_2Fe_{16}Ga_{0.5}TM_{0.5}$ as a function of TM atomic number.

Table 2. Atomic site occupancy derived from Rietveld refinement for Gd_2Fe_{17} and $Gd_2Fe_{16}Ga_{0.5}TM_{0.5}$ (TM = Cr, Mn, Co, Ni, Cu, Zn, and Ga).

TM	*Gd1*(*2b*)	*Gd2*(*2d*)	*Fe*(*4f*)	*Fe*(*6g*)	*Fe*(*12j*)	*Fe*(*12k*)	*Ga*(*4f*)	*Ga*(*6g*)	*Ga*(*12j*)	*Ga*(*12k*)	*TM*(*4f*)	*TM*(*6g*)	*TM*(*12j*)	*TM*(*12k*)
Cr	0.0861	0.0809	0.1581	0.2360	0.4580	0.4956	0.0047	0.0068	0.0148	0.0112	0.0072	0.0032	0.0159	0.0181
Mn	0.0829	0.0846	0.1510	0.2327	0.4379	0.5017	0.0042	0.0061	0.0128	0.0108	0.0082	0.0041	0.0166	0.0188
Fe	0.0854	0.0815	0.1706	0.2580	0.4973	0.5293								
Co	0.0835	0.0827	0.1509	0.2410	0.4589	0.4891	0.0057	0.0118	0.0112	0.0115	0.0047	0.0093	0.0144	0.0157
Ni	0.0861	0.0809	0.1518	0.2527	0.4323	0.4824	0.0081	0.0117	0.0062	0.0171	0.0069	0.0103	0.0147	0.0162
Cu	0.0839	0.0821	0.1503	0.2435	0.4521	0.4803	0.0052	0.0121	0.0118	0.0109	0.0051	0.0083	0.0151	0.0169
Zn	0.0816	0.0839	0.1511	0.2321	0.4310	0.4956	0.0045	0.0058	0.0124	0.0102	0.0075	0.0042	0.0179	0.0129
Ga	0.0812	0.0836	0.1455	0.2314	0.4285	0.4863	0.0094	0.01938	0.0309	0.0341				

The Fe–Fe site-to-site bond distances are listed in Table 3 and are plotted in Figure 3. It can be observed in Table 3 that the 4*f*-4*f* bond distances are smallest (~2.40 Å), and 12*k*-12*k* (2.46 Å) and 12*j*-12*j* (2.57 Å) distances are greatest of all. Other bond distances such as 6*g*-12*j*, 6*g*-12*k*, and 12*k*-12*k* have values close to 2.45 Å and do not show much variation with TM doping. It is to be noted that because of the aforementioned variation in bond distances, it is highly unlikely that these bond-length changes will have a drastic effect on the Curie temperature of the compounds. In fact, a slight reduction in bond distances is observed up to Cu substitution, which ideally should lead to an increase in antiferromagnetic exchange coupling between Fe–Fe moments and hence Curie temperature reduction. The observed changes in bond distances are in line with the metallic radii of the TM atoms (Figure 2).

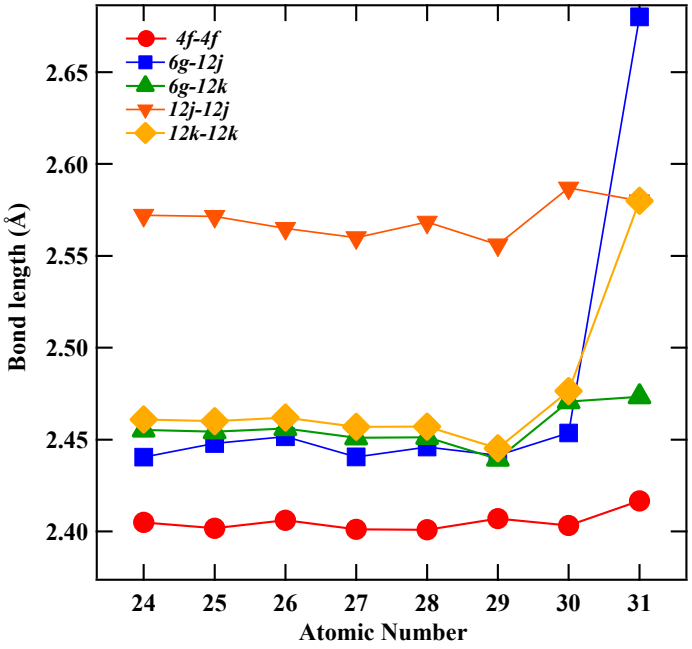

Figure 3. Atomic site–site bond lengths as a function of TM atomic number in $Gd_2Fe_{16}Ga_{0.5}TM_{0.5}$ (TM = Cr, Mn, Co, Ni, Cu, Zn, and Ga) derived from Rietveld refinement.

Table 3. Interatomic Fe–Fe distances (in Å) for Gd_2Fe_{17} and $Gd_2Fe_{16y}Ga_{0.5}TM_{0.5}$ (TM = Cr, Mn, Co, Ni, Cu, Zn, and Ga) obtained from Rietveld refinement.

Fe–Fe Sites	Cr	Mn	Fe	Co	Ni	Cu	Zn	Ga
4*f*-4*f*	2.4050(4)	2.4018(13)	2.4061(3)	2.4012(5)	2.4010(11)	2.4070(3)	2.4032(2)	2.4166(21)
6*g*-12*j*	2.4405(9)	2.4479(9)	2.4516(2)	2.4406(16)	2.4460(3)	2.4414(7)	2.4536(3)	2.6801(3)
6*g*-12*k*	2.4552(13)	2.4543(5)	2.4560(2)	2.4510(7)	2.4513(3)	2.4394(11)	2.4707(2)	2.4734(3)
12*j*-12*j*	2.5721(3)	2.5715(2)	2.5650(1)	2.5600(7)	2.5684(2)	2.5561(2)	2.587(21)	2.5800(3)
12*k*-2*k*	2.4610(13)	2.4600(13)	2.4620(4)	2.4570(2)	2.4571(11)	2.4453(11)	2.4764(11)	2.5800(12)

RT magnetization vs. field plot for $Gd_2Fe_{16}Ga_{0.5}TM_{0.5}$ is shown in Figure 4. The RT magnetic parameters derived from the hysteresis curves are plotted in Figure 5 and are listed in Table 4. The "law of approach" to saturation magnetization was used to determine the saturation magnetization, *Ms*. The law of approach describes the relationship between magnetization M on the applied magnetic field for H greater than coercive field *Hc*. The magnetization near *Ms* can be written as [27], $M = Ms\left(1 - \frac{a}{H} - \frac{b}{H^2}\right) + \kappa H$, where M is the magnetization, H is the applied magnetic field, and M_S is the saturation magnetization attained at a high field. The term κH represents the field-induced increase in the spontaneous magnetization of the domains. This term is very small at a temperature well below the Curie temperature and could be neglected. The term "*a*" is generally interpreted as due to microstress and ignored in the high field region, and "*b*" as due to crystal anisotropy. Where magneto-crystalline is a dominant term, a plot of M vs. $1/H^2$ in the high field region gives a straight line, the intercept of

which (with the *M*-axis) gives the *Ms* and the slope of which gives the magneto-crystalline anisotropy constant. Interesting variation in *Ms* is noticed with the TM atom doping. The *Ms* was observed to decrease first with Cr and Mn doping and then increase with TM atomic number up to Cu, and it decreased for Zn and Ga doping. The highest Ms ~77 emu/g was observed with Cu doping in $Gd_2Fe_{16}Ga_{0.5}TM_{0.5}$, while a low *Ms* was observed upon Cr (60 emu/g), Mn (57 emu/g), and Zn (59 emu/g) doping. As compared to Gd_2Fe_{17} (67 emu/g), $Gd_2Fe_{16}Ga_{0.5}Cu_{0.5}$ (77 emu/g) showed an increase of 15% in the *Ms* value. The observed variation in Ms can be attributed to the Fe(3d)-TM(3d) hybridization effect of orbitals. The extent of Fe(3d)-3d hybridization raises or lowers the bandwidth, which eventually changes the magnetic moment of Fe atoms [28,29]. The electronic configuration of TM atoms is Cr ([Ar]$4s^1 3d^5$), Mn [Ar]$4s^2 3d^5$, Fe [Ar]$4s^2 3d^6$, Co [Ar]$4s^2 3d^7$, Ni [Ar]$4s^2 3d^8$, Cu [Ar]$4s^1 3d^{10}$, Zn [Ar]$4s^2 3d^{10}$, and Ga [Ar] $4s^2$ $4p^1 3d^{10}$). In the case of early transition metals, 3d states are positioned at higher energies than those of Fe. Due to exchange splitting, 3d↓ spin-down states moved up in energy and were therefore close to the 3d states of early transition metals. Thus, the hybridization of 3d states of early transition metals is stronger with 3d↓ spin-down states than with 3d↑ spin-up states of Fe. As a result, the fraction of spin down 3d↓ states of early transition metals found in the energy region of Fe–3d is increased. Since the Fermi level is situated in this region, anti-ferromagnetic coupling follows. For the late transition metals, the situation is reversed, and ferromagnetic coupling follows [30–32]. Given this explanation, Cr- and Mn-doped $Gd_2Fe_{16}Ga_{0.5}TM_{0.5}$ show lower magnetization while Co-, Ni-, and Cu-doped samples show increasingly higher magnetization. A rather rapid decrease in *Ms* has been reported in $Er_2Fe_{17-x}Mn_x$ with increasing Mn content and has been attributed to the antiferromagnetic coupling between Fe and Mn [33]. The lower magnetization values of Zn and Ga results from the magnetic dilution effect upon replacing magnetic Fe with non-magnetic Zn and Ga atoms.

Table 4. Room temperature saturation magnetization, *Ms*, and Curie temperature, *Tc*, of Gd_2Fe_{17} and $Gd_2Fe_{16}Ga_{0.5}TM_{0.5}$ (TM = Cr, Mn, Co, Ni, Cu, Zn, and Ga).

$Gd_2Fe_{16}Ga_{0.5}TM_{0.5}$	*Ms* (emu/g)	*Tc* (K)
Cr	59.78	571
Mn	56.75	526
Gd_2Fe_{17}	67.00	513
Co	68.61	587
Ni	72.61	557
Cu	76.79	570
Zn	59.04	537
$Gd_2Fe_{16}Ga_1$	67.49	559

The measured Curie temperature, *Tc*, of $Gd_2Fe_{16}Ga_{0.5}TM_{0.5}$ compounds is plotted in Figure 5 as a function of TM atomic number. It is evident from Figure 5 that the TM doping affects the *Tc* of $Gd_2Fe_{16}Ga_{0.5}TM_{0.5}$ compounds. The Curie temperature reaches a maximum value of 587 K for Co doping followed by a reduction in *Tc* with increasing TM atomic number. A 15% increase in *Tc* was observed upon Co doping in $Gd_2Fe_{16}Ga_{0.5}TM_{0.5}$ as compared to that of Gd_2Fe_{17} (513 K) and a 4% increase as compared to $Gd_2Fe_{16}Ga$ (559K). In the Fe-rich R_2Fe_{17} intermetallic, the *Tc* is mainly determined by the strength and number of Fe–Fe exchange interactions. The strength of Fe–Fe exchange interaction is strongly dependent on the interatomic Fe–Fe distances described [9,34–36]. Accordingly, the exchange interactions between iron atoms situated at distances smaller (greater) than 2.45−2.50 Å are negative (positive). In the R_2Fe_{17} majority of Fe–Fe, distances favor a negative interaction [37]. The negative exchange interaction can be reduced either by volume expansion or by reducing the number of Fe–Fe pairs with negative exchange interactions. The low T_C observed in parent Gd_2Fe_{17} compound is believed to be due to the short Fe–Fe interatomic distances found at the 4*f*(6*c*) sites in the hexagonal (rhombohedral) structure, which couple antiferromagnetically since their separation is ~2.4 Å (Figure 3), which is less than 2.45 Å needed for ferromagnetic ordering [38].

It is to be noted that the increase in *Tc* has been reported earlier with higher Al, Ga, and Si content (at x > 2) in $R_2Fe_{17-x}M_x$ (M = Al, Ga, and Si) [15] but with a concomitant reduction in *Ms* due to large Fe replacement with non-magnetic atoms. A *Tc* value of 581 K has been reported earlier in the $YGdFe_{16}CoGa$ [39] compound, but a reported *Tc* ~586 K of $Gd_2Fe_{16}Ga_{0.5}Co_{0.5}$ exceeds that of the former compounds. Thus, the observed increase in *Tc* in TM-doped $Gd_2Fe_{16}Ga_{0.5}TM_{0.5}$ compounds is highest with a minimum replacement of Fe atoms.

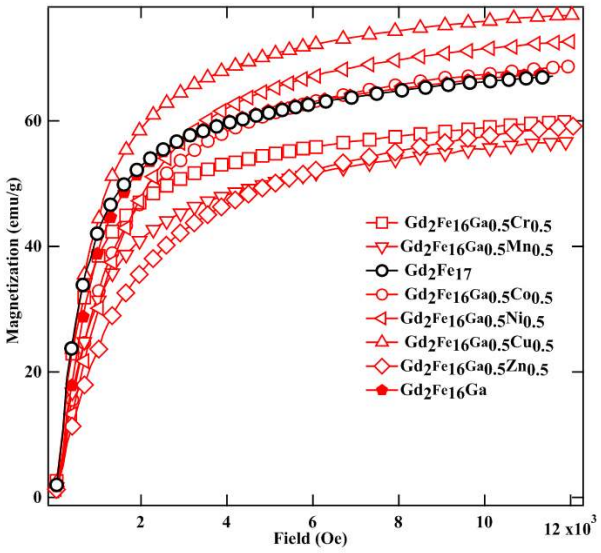

Figure 4. Room temperature M vs. H plot of Gd_2Fe_{17} and $Gd_2Fe_{16}Ga_{0.5}TM_{0.5}$ (TM = Cr, Mn, Co, Ni, Cu, Zn, and Ga).

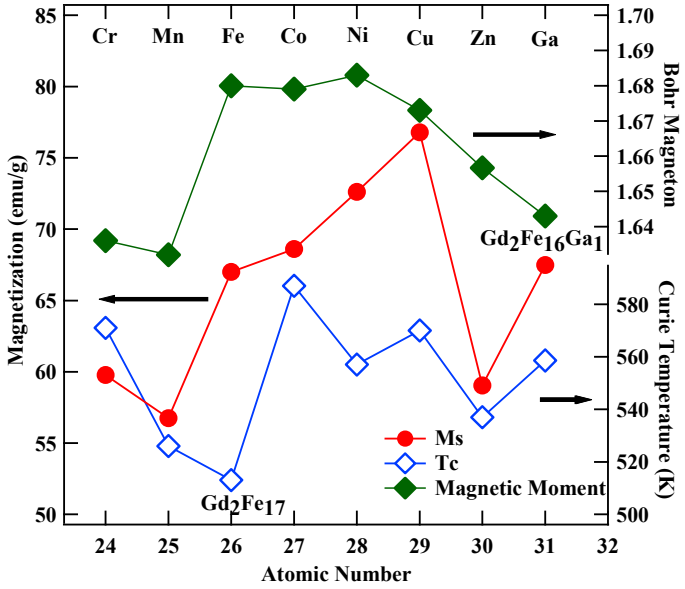

Figure 5. Saturation magnetization, *Ms*, Curie temperature, *Tc*, and Bohr magneton number as a function of TM atomic number in Gd_2Fe_{17} and $Gd_2Fe_{16}Ga_{0.5}TM_{0.5}$ (TM = Cr, Mn, Co, Ni, Cu, Zn, and Ga).

The Friedel model [40] can also be used to explain the observed variation in *Tc*. According to this model, the strength of interaction between two magnetic moments would be strong and ferromagnetic, if $\lambda/d > 1$, where distance "*d*" between these magnetic atoms is smaller than the distance "λ" covered by the main peak of the Friedel oscillations. In compounds containing 3d transition metals, it has been established that the magnetic coupling is governed mainly by the NN interactions and is proportional

to the lattice parameters. Furthermore, λ is found to be inversely proportional to the Fermi wave vector, k_f. For the 3d band in the R_2Fe_{17} compounds, k_f is large. Substitution of TM decreases the holes in the 3d-band and hence decreases k_f. The substitution of Ga leads to lattice expansion and hence increases "*d*", which will have an effect of reducing the λ/d ratio. Since the substitution of Co, Ni, and Cu brings in lattice volume reduction as compared to $R_2Fe_{16}Ga$; there is hence an increase in the $\lambda/d > 1$ and *Tc* [39,40]. The reported theoretical studies attribute changes in the Curie temperature in substituted $R_2Fe_{17-x}T_x$ (T = Al, Si, Ga, and Ti) intermetallic to be electronic in origin other than due to the simple volume expansion effect and hence bond distances [41–43]. The effect of the substitution is to fill out the Fe–3d spin-up sub-bands, which alter the magnetic moment of the compound and hence the strength of exchange interaction [41,44]. In fact, theoretical calculations performed using the LSDA+U method showed enhancement between Fe–Fe atoms in the presence of Ga in $Gd_2Fe_{17-x}Ga_x$ compounds, which in turn was shown to enhance *Tc* for low Ga (x < 3) content [45]. Thus, the higher *Tc* values of $Gd_2Fe_{16}Ga_{0.5}TM_{0.5}$ as compared to that of pure Gd_2Fe_{17} could be attributed to this effect as well. In comparison to various doped intermetallic such as $Gd_2Fe_{16}Ga$ (~410 K) [46], $Gd_2Fe_{16}Ga_{0.5}Ti_{0.5}$ (556 K) [47], $Dy_2Fe_{16}Ga$ (~462 K) [8], $Ce_2Fe_{16}Ga$ (~320 K) [48], $Sm_2Fe_{16}Ga$ (~505 K) [49], or $Sm_2Fe_{16.2}Ti_{0.8}$ (~435 K) [50], the reported compound $Gd_2Fe_{16}Ga_{0.5}TM_{0.5}$ with Co, Ni, and Cu substitution certainly exhibits higher *Tc* and *Ms*, thus ensuring their potential use as high-temperature permanent magnet applications.

The room temperature (RT) Mössbauer spectra for $Gd_2Fe_{16}Ga_{0.5}TM_{0.5}$ are shown in Figure 6. The intermetallic R_2Fe_{17} with a Th_2Ni_{17} structure have the easy direction of magnetization and hyperfine field lying in the basal plane along the *a* or *b* axes of the unit cell [51,52]. This easy basal plane direction of magnetization complicates the Mössbauer spectral analysis of R_2Fe_{17} compounds because it involves four crystallographically inequivalent iron sites. The reason for the inequivalent iron site is the vector character of the hyperfine field and tensor character of the electric field gradient [53]. Thus, this inequivalency demands further magnetic splitting of g, *j*, and *k* iron sites. Mössbauer studies of $Gd_2Fe_{16}Ga_{0.5}TM_{0.5}$ have been conducted accordingly, either with 8 or 10 magnetic sextets, with an absence or presence of impurity phase, respectively [48,54–56]. The Mössbauer spectral analysis was carried out with magnetic sextets assigned to the 4*f*, 6*g*, 12*j*, and 12*k* sites in Gd_2Fe_{17}. The 6*g*, 12*j*, and 12*k* sites were further split into 2, 3, and 2 corresponding to the site occupancies of Fe atoms in the crystal structure of R_2Fe_{17} with the planar anisotropy. The intensities of the six absorption lines of each sextet were assumed to follow the 3:2:1 intensity ratio expected for randomly oriented powder samples in zero magnetic fields and a single common line-width was assumed for all eight sextets. The isomer shifts (IS, δ) for the magnetically inequivalent sites were constrained to be the same, whereas the hyperfine field (HF, B_{hf}) was expected to vary at pairs of magnetically inequivalent sites due to variations in the dipolar and orbital contributions to the magnetic hyperfine fields [57]. The ^{57}Fe Mössbauer spectra show hyperfine split sextets in $Gd_2Fe_{16}Ga_{0.5}TM_{0.5}$, revealing that the samples are magnetically ordered, and all of them have different sub-spectra with different magnetic hyperfine fields.

The hyperfine parameters derived from the fitting are listed in Table 5, and weighted average (Wt.Avg.) hyperfine field (HF) and isomer shifts (IS, δ) are plotted in Figure 7. There exists a direct correlation between hyperfine field values of a site to its near neighbor (NN) iron sites. In case of Th_2Ni_{17} structure, 12*k* site has 9 NN Fe sites (1(4*f*), 2(6*g*), 4(12*j*), 2(12*k*)), *12j* has 10 NN Fe sites (2(4*f*), 2(6*g*), 2(12*j*), 4(12*k*)), 6*g* has 10 NN Fe sites (2(4*f*), 0(6*g*), 4(12*j*), 4(12*k*)), and 4*f* site has 11 NN Fe sites (1(4*f*), 3(6*g*), 6(12*j*), 3(12*k*)). Following the NN distribution, the observed HF values are in 4*f*(6*c*) > 12*j*(18*f*) > 6*g*(9*d*) > 12*k*(18*h*) sequence, which is similar to the sequence observed in other R_2Fe_{17} compounds [58,59]. It is obvious that 4*f* (6*c*) site has the maximum hyperfine field, since it has the maximum number of Fe nearest neighbors, whereas, the 18*h* (12*k*) site has the minimum number of Fe neighbors and consequently has the least HF value. Although 6*g*(9*d*) and 12*j*(18*f*) sites have the same number of Fe neighbors, the former has comparatively smaller Fe-Fe distances, and hence a larger hyperfine field, Tables 3 and 5. The Cu and Mn-doped $Gd_2Fe_{16}Ga_{0.5}TM_{0.5}$ display a low

Wt. Avg. HF values as compared to other TM doped $Gd_2Fe_{16}Ga_{0.5}TM_{0.5}$ compounds. The Wt. Avg. HF value reaches the maximum for Gd_2Fe_{17} and $Gd_2Fe_{16}Ga_{0.5}Co_{0.5}$, to a value ~252 kOe followed with a gradual decline in its value, reaching a value of 246 kOe for $Gd_2Fe_{16}Ga_1$. This decrease in HF value results from the decreased magnetic exchange interactions resulting from Fe replacement with non-magnetic Cu, Zn, and Ga atoms. Furthermore, under the first approximation, the hyperfine field is assumed proportional to the magnetic moment. We obtained the Fe moment using the hyperfine coupling constant of 150 kOe/μB, which has been reported for Y–Fe systems [60,61]. The average value of Fe magnetic moment for $Gd_2Fe_{16}Ga_{0.5}TM_{0.5}$ is plotted in Figure 5. In general, Fe magnetic moment holds up to the value of 1.68 μB only for Fe, Co, and Ni substitution in $Gd_2Fe_{16}Ga_{0.5}TM_{0.5}$.

The isomer shift values were assigned in relation to the Wigner–Seitz cell volume, i.e., the greater the Wigner–Seitz cell volume, the greater the isomer shift (Table 5) [62]. Therefore, as V(4*f*) > V(12*j*)~V(12*k*) > V(6*g*), their corresponding IS is as follows: $\delta 4f > \delta 12j \sim \delta 12k > \delta 6g$. The room temperature values of Wt.Avg. IS for $Gd_2Fe_{16}Ga_{0.5}TM_{0.5}$ are negative, and the magnitudes of IS increase with an increasing TM atomic number in $Gd_2Fe_{16}Ga_{0.5}TM_{0.5}$. The IS is proportional to the total *s*-electron charge density at the iron nucleus, which is the sum of the spin-up and spin-down *s*-electron density and lattice site volume; an increasing *s*-electron density at the iron nucleus is indicated by a decreasing isomer shift. The observed behavior of the IS value could be attributed to the competition between lattice site volume and the complex nature of hybridization in Fe–Ga–TM [63,64], which all affect the *s*-electron charge density at the iron nucleus. A volume contraction is observed until TM = Ni, followed by unit cell expansion until TM = Zn doping in $Gd_2Fe_{16}Ga_{0.5}TM_{0.5}$. However, the Wt.Avg. IS value becomes less negative with TM = Co and onward. Thus, this behavior of IS indicates electronic effects at play in dictating IS behavior of the $Gd_2Fe_{16}Ga_{0.5}TM_{0.5}$ compound. The increased IS value with Co, Ni, Cu, Zn, and Ga in $Gd_2Fe_{16}Ga_{0.5}TM_{0.5}$ could be associated with the increased number of the 3d electrons, which increases the shielding of the *s*-electrons from the nucleus. In earlier TM atoms viz. Cr and Mn, the 3d band is broader and heavily hybridized with the conduction band [40]. These make electrons freer and thus have a greater presence at the Fe nucleus, which makes IS more negative. The increased screening of *s*-electrons via 3d electrons beyond TM = Fe doping in $Gd_2Fe_{16}Ga_{0.5}TM_{0.5}$ could be the reason for enhanced IS.

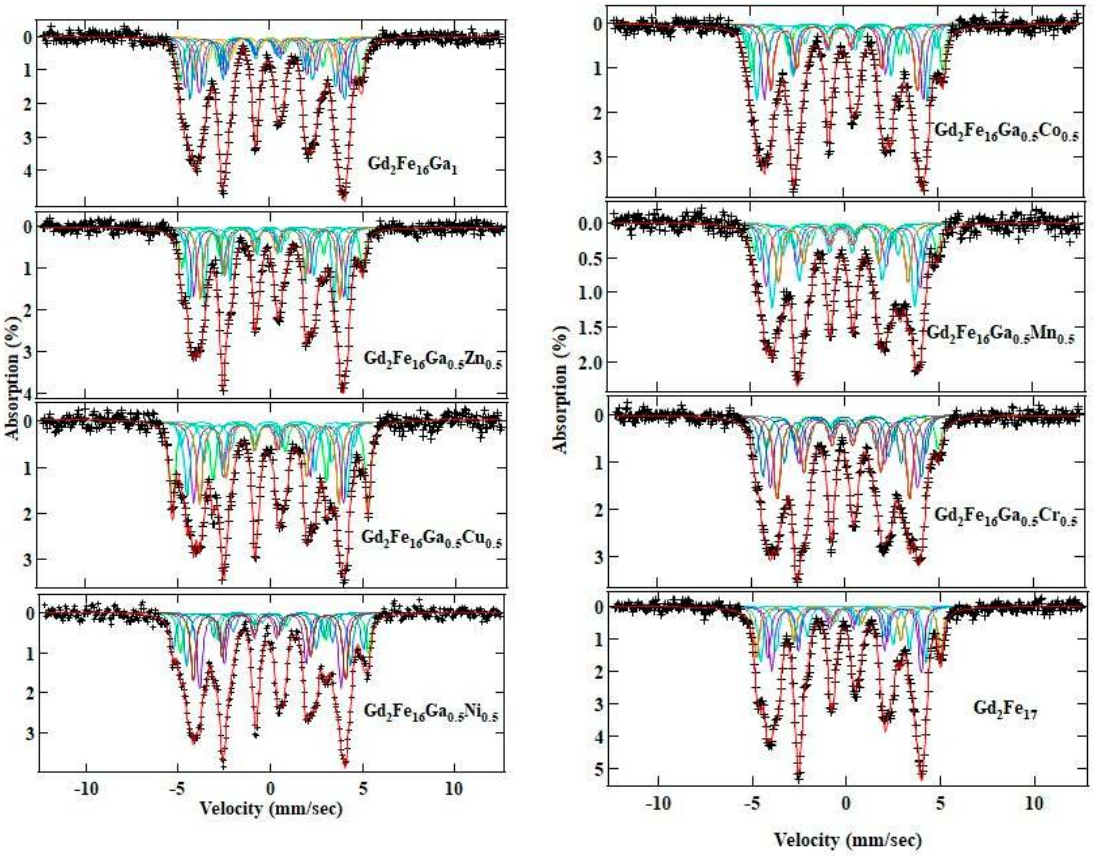

Figure 6. Fitted RT Mössbauer spectra of Gd_2Fe_{17} and $Gd_2Fe_{16}Ga_{0.5}TM_{0.5}$ (TM = Cr, Mn, Co, Ni, Cu, Zn, and Ga).

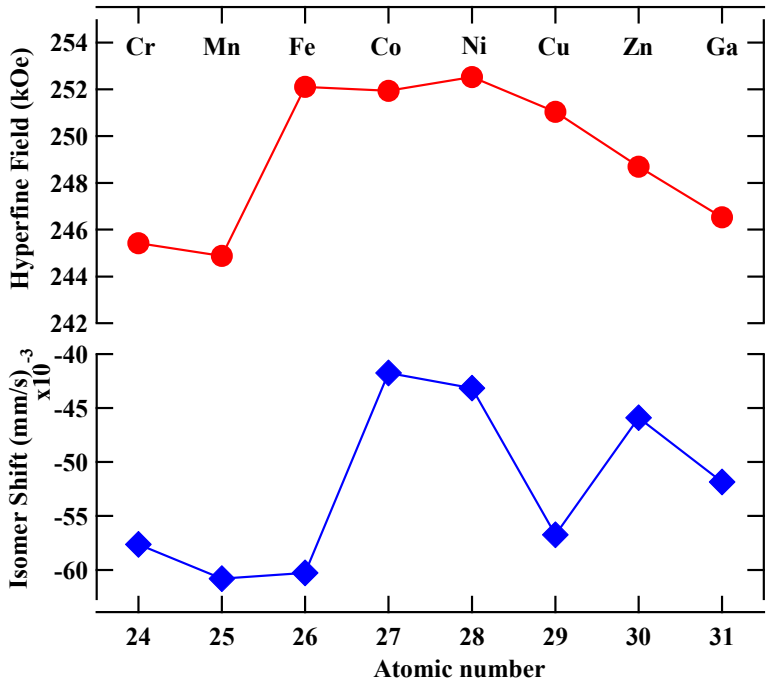

Figure 7. Weighted average hyperfine parameters, hyperfine field, and isomer shift, as a function of TM atomic number for Gd_2Fe_{17} and $Gd_2Fe_{16}Ga_{0.5}TM_{0.5}$ (TM = Cr, Mn, Co, Ni, Cu, Zn, and Ga).

Table 5. RT Mössbauer hyperfine parameters for Gd_2Fe_{17} and $Gd_2Fe_{16}Ga_{0.5}TM_{0.5}$ (TM = Cr, Mn, Co, Ni, Cu, Zn, and Ga).

TM		4*f*	6g_1	6g_2	12j_1	12j_2	12j_3	12k_1	12k_2	Doublet	Wt.Avg.
Cr	B (kOe)	303	231.6	244.1	212.5	271.2	278.5	198	255.3		245.424
	IS (mm/s)	0.102	−0.121	−0.121	−0.1	−0.1	−0.1	0.011	0.011		−0.0576
	QS (mm/s)	0.351	0.116	0.162	0.073	−0.157	−0.009	0.35	−0.0446		
	Area (%)	10.0	15.2	17.8	12.5	4.3	18.5	9.9	11.7		
Mn	B (kOe)	302.3	230	254.3	210.1	265.2	275.1	202	255.6		244.882
	IS (mm/s)	0.078	−0.117	−0.117	−0.124	−0.124	−0.124	0.039	0.039		−0.0608
	QS (mm/s)	0.28	0.093	0.093	−0.157	0.149	−0.079	0.434	−0.17		
	Area (%)	8.2	16.3	17.6	8.7	23.1	10.6	10.7	6.2		
(Gd_2Fe_{17})	B (kOe)	304	246.2	254.6	220.5	272.3	286.3	205.6	260.2		252.1
	IS (mm/s)	0.07	−0.13	−0.13	−0.115	−0.115	−0.115	0.035	0.035		−0.0603
	QS (mm/s)	0.067	0.296	0.21	−0.019	0.009	−0.116	0.358	−0.487		
	Area (%)	13.8	15.5	19.8	6.1	13.6	11.9	6.16	11.7		
Co	B (kOe)	315.2	242.7	262.9	215.6	271.3	283	203.2	264.6		251.932
	IS (mm/s)	0.11	−0.119	−0.119	−0.098	−0.098	−0.098	0.056	0.056		−0.0417
	QS (mm/s)	0.139	0.272	0.238	−0.399	0.015	−0.039	0.263	−0.245		
	Area (%)	11.5	16	18.1	7.1	18.4	5.9	10.1	10.8		
Ni	B (kOe)	310.1	239.1	257.4	220.6	276.7	285.2	201.9	263.3	44.4	252.524
	IS (mm/s)	0.113	−0.129	−0.129	−0.09	−0.09	−0.09	0.044	0.044	0.5	−0.0432
	QS (mm/s)	0.265	0.458	0.055	−0.036	0.042	−0.079	0.138	0.151	−0.5	
	Area (%)	11.0	3.5	9.3	8.0	18.6	8.3	14.3	16.6	8.4	
Cu	B (kOe)	312.2	234.5	252.1	214.8	269.2	290.3	200.2	268.0	45.9	251.032
	IS (mm/s)	0.113	−0.137	−0.137	−0.128	−0.128	−0.128	0.062	0.062	0.387	−0.0567
	QS (mm/s)	0.021	0.172	0.102	−0.005	−0.083	−0.103	−0.358	−0.17	−0.39	
	Area (%)	22.0	20.8	20.4	10.3	18.7	6.5	1.9	2.6	2.8	
Zn	B (kOe)	303.4	234.5	252.3	217.1	265.0	280.7	211.3	256.4		248.689
	IS (mm/s)	0.088	−0.141	−0.141	−0.101	−0.101	−0.101	0.062	0.062		−0.0459
	QS (mm/s)	0.041	0.252	0.125	0.098	−0.0001	−0.033	0.178	−0.145		
	Area (%)	11.3	19.4	18.8	13.2	19.5	4.3	3.4	9.1		
Ga	B (kOe)	304.8	235.6	238.3	222.8	255.1	283.8	208.2	252.9		246.529
	IS (mm/s)	0.059	−0.109	−0.109	−0.113	−0.113	−0.113	0.05	0.05		−0.0518
	QS (mm/s)	0.025	−0.086	0.211	0.216	0.275	−0.023	0.093	−0.147		
	Area (%)	12.3	14.0	15.3	13.5	11.7	17.3	6.8	9.9		

4. Conclusions

The effect of double substitution of Ga and TM in $Gd_2Fe_{16}Ga_{0.5}TM_{0.5}$ on structural and magnetic properties was compared with Gd_2Fe_{17} compounds. These compounds were found to crystallize in a hexagonal Th_2Ni_{17} structure. Lattice parameters and unit cell volume of TM-doped $Gd_2Fe_{16}Ga_{0.5}TM_{0.5}$ compounds showed dependence on the atomic radii of the TM dopant. The variance of the *c*/*a* ratio with the substation in these compounds showed anisotropic unit cell volume expansion. The Rietveld analysis showed the preferred occupancy of TM for 12*k* and Ga for 12*k* and 12*j* sites. Overall, no direct correlation was observed between the trend in Curie temperature and bond distances. The observed *Tc* reached a maximum value of 587 K for cobalt substitution, which is 15% higher than the *Tc* value of Gd_2Fe_{17}. Furthermore, 15% and 14% enhancement in *Ms* was observed for Cu-substituted $Gd_2Fe_{16}Ga_{0.5}TM_{0.5}$ compound as compared to Dy_2Fe_{17} and $Dy_2Fe_{16}Ga_1$ compounds, respectively. Furthermore, unlike other doped compounds of intermetallic $RE_2Fe_{17-x}M_x$ (M = Al, Si, Ga), where improvements in *Tc* is compromised with the reduction in *Ms*, in the present studied compound $Gd_2Fe_{16}Ga_{0.5}TM_{0.5}$, even small TM doping (TM = Co, Ni, and Cu) brought about a simultaneous enhancement in *Ms* and *Tc*. The combined magnetic and Mössbauer study points to the fact that the observed improvement in *Tc* and *Ms* could be attributed to electronic effects resulting from Fe–3d hybridization with a substituted TM atom electronic shell. A concomitant improvement in *Ms* and *Tc* is desirable for the magnetic industry. The study elucidates that the judicious selection of dopants and its content can improve the *Ms* and *Tc* of the R_2Fe_{17} intermetallic compounds.

Author Contributions: Data Curation, Methodology and writing original draft preparation, J.N.D.; Revising/Editing the original draft, S.R.M.; Rietveld analysis, K.S.S.A.; Revising the paper, J.A.

Funding: This research was funded by NSF-CMMI (Grant #: 1029780) and NSF-TN-SCORE (Grant #: EPS-10004083).

Conflicts of Interest: The authors declare no conflict of interest.

References

1. National Imports LLC. *Permanent Magnet Selection and Design Handbook*; Magcraft, Advance Magnetic Materials: Vienna, VA, USA, 2007.
2. Strnat, K.J. Chapter 2—Rare earth-cobalt permanent magnets. *Handb. Ferromagn. Mater.* **1988**, *4*, 131–209.
3. Coey, J.M.D.; Sun, H. Improved magnetic properties by treatment of iron-based rare earth intermetallic compounds in ammonia. *J. Magn. Magn. Mater.* **1990**, *87*, L251. [CrossRef]
4. Coey, J.M.D.; Sun, H.; Otani, Y.; Hurley, D.P.F. Gas-phase carbonation of R_2Fe_{17}; R = Y, Sm. *J. Magn. Magn. Mater.* **1991**, *98*, 76–78. [CrossRef]
5. Zhong, X.P.; Radwanski, R.J.; de Boer, F.R.; Jacobs, T.H.; Buschow, K.H.J. Magnetic and crystallographic characteristics of rare-earth ternary carbides derived from R_2Fe_{17} compounds. *J. Magn. Magn. Mater.* **1990**, *86*, 333–340. [CrossRef]
6. Buschow, K.H.J.; Coehoorn, R.; de Mooij, D.B.; de Waard, K.; Jacobs, T.H. Structure and magnetic properties of $R_2Fe_{17}Nx$ compounds. *J. Magn. Magn. Mater.* **1990**, *92*, L35. [CrossRef]
7. Xu, R.; Zhen, L.; Yang, D.; Wu, J.; Wang, X.; Wang, Q.; Chen, C.; Dai, L. Effect of Ga on the structural stablity of $Sm_2(FeGa)_{17}$ compounds. *Mater. Lett.* **2002**, *57*, 146. [CrossRef]
8. Shen, B.G.; Cheng, Z.H.; Gong, H.Y.; Liang, B.; Yan, Q.W.; Zhan, W.S. Magnetic anisotropy of $Dy_2Fe_{17-x}Gax$ compounds. *Solid State Commun.* **1995**, *95*, 813–816. [CrossRef]
9. Givord, D.; Lemaire, R. Magnetic transition and anomalous thermal expansion in R_2Fe_{17} compounds. *IEEE Trans. Magn.* **1974**, *10*, 109–113. [CrossRef]
10. Jacobs, T.H.; Buschow, K.H.J.; Zhou, G.F.; Li, X.; de Boer, F.R. Magnetic interactions in $R_2Fe_{17-x}Alx$ compounds (R = Ho, Y). *J. Magn. Magn. Mater.* **1992**, *116*, 220–230. [CrossRef]
11. Shen, B.G.; Wang, F.W.; Kong, L.S.; Cao, L. Magnetic anisotropy of $Sm_2Fe_{17-x}Gax$ compounds with $0 \leq x \leq 6$. *J. Phys. Condens. Matter* **1993**, *5*, L685. [CrossRef]
12. Sun, H.; Coey, J.M.D.; Otani, Y.; Hurley, D.P.F. Magnetic properties of a new series of rare-earth iron nitrides: $R_2Fe_{17}Ny$(y approximately 2.6). *J. Phys. Condens. Matter* **1990**, *2*, 6465. [CrossRef]

13. De Mooij, D.B.; Buschow, K.H.J. Formation and magnetic properties of the compounds $R_2Fe_{14}C$. *J. Less-Common Met.* **1988**, *142*, 349–357. [CrossRef]
14. Lukoyanov, A.V.; Kokorina, E.E.; Medvedev, M.V.; Nekrasov, I.A. Ab initio exchange interactions and magnetic properties of Gd_2Fe_{17} iron sublattice: Rhombohedral vs. hexagonal phases. *Phys. Rev. B* **2009**, *80*, 104409. [CrossRef]
15. Rao, K.V.S.R.; Ehrenberg, H.; Markandeyulu, G.; Varadaraju, U.V.; Venkatesan, M.; Suresh, K.G.; Murthy, V.S.; Schmidt, P.C.; Fuess, H. On the Structural and Magnetic Properties of $R_2Fe_{17-x}(A,T)_x$ (R =Rare Earth; A Al, Si, Ga; T= Transition Metal)Compounds. *Phys. Status Solid (a)* **2002**, *189*, 373–388. [CrossRef]
16. Coey, J.M.D. New permanent magnets; manganese compounds. *J. Phys. Condens. Matter* **2014**, *26*, 064211. [CrossRef] [PubMed]
17. Rietveld, H.M. A profile refinement method for nuclear and magnetic structures. *J. Appl. Cryst.* **1969**, *2*, 65–71. [CrossRef]
18. Petříček, V.; Dušek, M.; Palatinus, L. Crystallographic Computing System JANA2006: General features. *Z. Kristallogr.* **2014**, *229*, 345. [CrossRef]
19. Liao, L.X.; Altounican, Z.; Ryan, D.H. Cobalt site preferences in iron rare-earth-based compounds. *Phy. Rev. B* **1993**, *47*, 11230–11241. [CrossRef]
20. Howard, C.J. The approximation of asymmetric neutron powder diffraction peaks by sums of Gaussians. *J. Appl. Crystallogr.* **1982**, *15*, 615–620. [CrossRef]
21. Pitschke, W.; Hermann, H.; Mattern, N. The influence of surface roughness on diffracted X-ray intensities in Bragg–Brentano geometry and its effect on the structure determination by means of Rietveld analysis. *Powder Diffr.* **1993**, *8*, 74–83. [CrossRef]
22. Yang, Q.W.; Yan, Q.W.; Zhang, P.L.; Shen, B.G.; Lang, F.W.; Kong, L.S.; Gou, C.; Chen, D.F.; Cheng, Y.F. A neutron powder diffraction study of the structure of $Ho_2Fe_{17-x}GaxC_2$ (x = 4.0 and 5.5). *J. Phys. Condens. Mater.* **1994**, *6*, 3567–3572.
23. Hu, Z.; Yelon, W.B.; Mishra, S.; Long, G.J.; Pringle, O.A.; Middleton, D.P.; Buschow, K.H.J.; Grandjean, F. A magnetic, neutron diffraction, and Mössbauer spectral study of $Nd_2Fe_{15}Ga_2$ and the $Tb_2Fe_{17-x}Gax$ solid solutions. *J. Appl. Phys.* **1994**, *76*, 443. [CrossRef]
24. Morariu, M.; Rogalski, M.S. 57Fe Mössbauer study of $Y_2Fe_{16}M$ compounds and their nitrides with M = Ga, V. *Phys. Status Solidi A* **1994**, *141*, 223–230. [CrossRef]
25. Cadogan, J.M.; Li, H.S.; Margarian, A.; Dunlop, J.B. On the ternary intermetallic phases formed by $YFe_{12-x}Gax$ ($1 \leq x \leq 2$). *Mater. Lett.* **1993**, *18*, 39–43. [CrossRef]
26. Li, H.-S.; Suharyana; Cadogan, J.M.; Ju, B.-P.; Shen, B.-G.; Wang, F.-W.; Zhan, W.-S. A Mossbauer study of $Sm_2Fe_{14}Ga_3C_x$ (x=0–2.5). *IEEE Trans. Mag.* **1995**, *31*, 3716–3718.
27. Chikazumi, S.; Graham, C.D. *Physics of Ferromagnetism*, 2nd ed.; Oxford University Press: New York, NY, USA, 2009; Volume 94.
28. Huang, M.Z.; Ching, W.Y. Effects of Al substitution in Nd_2Fe_{17} studied by first principles calculations. *J. Appl. Phys.* **1994**, *76*, 7046. [CrossRef]
29. Huang, M.Z.; Ching, W.Y. First principles calculation of the electronic and magnetic properties of $Nd_2Fe_{17-x}Mx$ (M = Si, Ga) solid solutions. *J. Appl. Phys.* **1996**, *79*, 5545. [CrossRef]
30. Akai, M.; Akai, H.; Kanamori, J. Electronic Structure of Impurities in Ferromagnetic Iron. II. 3d and 4d Impurities. *J. Phys. Soc. Jpn.* **1985**, *54*, 4257–4264. [CrossRef]
31. Drittler, B.; Stefanou, N.; Blugel, S.; Zeller, R.; Dederichs, P.H. Electronic structure and magnetic properties of dilute Fe alloys with transition-metal impurities. *Phys. Rev. B* **1989**, *40*, 8203. [CrossRef]
32. Mirbt, S.; Eriksson, O.; Johansson, B.; Skriver, H.L. Magnetic coupling in 3d transition-metal monolayers and bilayers on bcc (100) iron. *Phys. Rev. B* **1995**, *52*, 15070. [CrossRef]
33. Wang, J.L.; Ibarra, M.R.; Marquina, C.; García-Landa, B.; Li, W.X.; Tang, N.; Wang, W.Q.; Yang, F.M.; Wu, G.H. Effect of Mn substitution on the volume and magnetic properties of Er_2Fe_{17}. *J. Appl. Phys.* **2002**, *92*, 1453. [CrossRef]
34. Neél, L. Propriétés magnétiques de l'état métallique et énergie d'interaction entre atomes magnétiques. *Ann. Phys.* **1936**, *5*, 232–279. [CrossRef]
35. Li, Z.W.; Morrish, A.H. Negative exchange interactions and Curie temperatures for Sm_2Fe_{17} and $Sm_2Fe_{17}Ny$. *Phys. Rev. B* **1997**, *55*, 3670. [CrossRef]

36. Dahal, J.N.; Wang, L.; Mishra, S.R.; Nguyen, V.V.; Liu, J.P. Synthesis and magnetic properties of $SrFe_{12-x-y}Al_xCoyO_{19}$ nanocomposites prepared via autocombustion technique. *J. Alloy. Comp.* **2014**, *595*, 213–220. [CrossRef]
37. Shen, B.G.; Cheng, Z.H.; Liang, B.; Guo, H.Q.; Zhang, J.X.; Gong, H.Y.; Wang, F.W.; Yan, Q.W.; Zhan, W.S. Structure and magnetocrystalline anisotropy of $R_2Fe_{17-x}Ga_x$ compounds with higher Ga concentration. *Appl. Phys. Lett.* **1995**, *67*, 1621. [CrossRef]
38. Valeanu, M.; Plugaru, N.; Burzo, E. Effect of nitrogenation on the magnetic properties of $Y_2Fe_{17-x}M_x$ compounds, with M = Al, Ga or Si. *Solid State Commun.* **1994**, *89*, 519–522. [CrossRef]
39. Srilatha, R.; Markandeyulu, G.; Murty, V. Effect of Co on the Magnetic Properties of $YGdFe_{17-x}Co_xGa$. *IEEE Trans. Magn.* **2006**, *42*, 917. [CrossRef]
40. Friedel, J.; Leman, G.; Olszewski, S. On the Nature of the Magnetic Couplings in Transitional Metals. *J. Appl. Phys. Suppl.* **1961**, *32*, 325S. [CrossRef]
41. Sabirianov, R.F.; Jaswal, S.S. Electronic structure and magnetism in $Sm_2Fe_{17-x}A_x$ (A = Al, Ga, Si). *J. Appl. Phys.* **1996**, *79*, 5942. [CrossRef]
42. Li, H.-S.; Coey, J.M.D. *Handbook of Magnetic Materials*; Buschow, K.H.J., Ed.; Elsevier: Amsterdam, The Netherlands, 1991; Volume 6, Chapter I, p. 1.
43. Ching, W.Y.; Huang, M.Z. Band Theoretical Investigation of Curie Temperatures of Modified R_2Fe_{17}-Based Intermetallic Compounds. *J. Appl. Phys.* **1996**, *79*, 4602. [CrossRef]
44. Hu, B.-P.; Li, H.-S.; Shen, B.-G.; Wang, F.-W.; Cadogan, J.M.; Zhan, W.-S. A 57Fe Mossbauer study of $Gd_2Fe_{17-x}Ga_xC_2$ (x = 0–6). *J. Appl. Phys.* **1996**, *79*, 5713. [CrossRef]
45. Kokorina, E.E.; Medvedev, M.V.; Nekrasov, I.A. Ab Initio Exchange Interactions and Magnetic Properties of Intermetallic Compound $Gd_2Fe_{17-x}Ga_x$. *Solid State Phenom.* **2010**, *168–169*, 196–199. [CrossRef]
46. Cheng, Z.H.; Shen, B.G.; Liang, B.; Zhang, J.X.; Wang, F.W.; Zhang, S.Y.; Zhao, J.G.; Zhan, W.S. Ga-concentration dependence of magnetocrystalline anisotropy in Gd_2Fe_{17-x}Gax Compounds. *J. Appl. Phys.* **1995**, *78*, 1385. [CrossRef]
47. Pokharel, G.; Ali, K.S.S.; Mishra, S.R. Structural, magnetic and Mossbauer studies of Ti doped $Gd_2Fe_{17-x}Ti_x$ and $Gd_2Fe_{16}Ga_{1-x}Ti_x$ ($0 \leq x \leq 1$). *J. Magn. Magn. Mater.* **2015**, *382*, 31–42. [CrossRef]
48. Long, G.J.; Mishra, S.R.; Pringle, O.A.; Hu, Z.; Yelon, W.B.; Grandjean, F.; Middleton, D.P.; Buschow, K.H.J. A magnetic, neutron diffraction, and Mossbauer spectral study of the Ce2Fe17-xGax solid solutions. *J. Magn. Magn. Mater.* **1997**, *176*, 217–232. [CrossRef]
49. Maruyama, F. Exchange interactions in $R_2Fe_{17-x}Ga_x$ (R =Y, Sm, Gd, Tb, Ho and Tm) compounds. *J. Solid State Chem.* **2005**, *178*, 3020–3026. [CrossRef]
50. Paoluzi, A.; Pareti, L. Magnetocrystalline anisotropy of Fe and Sm sublattices in Sm_2Fe_{17}: Effects of Ti substitution for Fe. *J. Mang. Magn. Mater.* **1998**, *189*, 89–95. [CrossRef]
51. Liao, L. Cobalt Site in Iron Rare-Earth Based Compounds. Ph.D. Thesis, McGill University, Montréal, QC, Canada, 1992.
52. Gubbens, P.C.M.; Buschow, K.H.J. Magnetic phase transition in Tm_2Fe_{17}. *J. Appl. Phys.* **1973**, *44*, 3739. [CrossRef]
53. Isnard, O.; Hautot, D.; Long, G.J.; Grandjean, F. A structural, magnetic, and Mössbauer spectral study of Dy_2Fe_{17} and its hydrides. *J. Appl. Phys.* **2000**, *88*, 2750. [CrossRef]
54. Buschow, K.H.J.; Wieringen, J.S.V. Crystal structure and magnetic properties of cerium-iron compounds. *Phys. Status Solidi* **1970**, *42*, 231–239. [CrossRef]
55. Levinson, L.M.; Rosenberg, E.; Shaulov, A.; Strnat, K. Mössbauer Study of Some 2–17 Lanthanide-Iron Compounds. *J. Appl. Phys.* **1970**, *41*, 910. [CrossRef]
56. Alp, E.E.; Umarji, A.M.; Malik, S.K.; Shenoy, G.K.; Huang, M.Q.; Boltich, E.B.; Wallace, W.E. 57Fe Mössbauer studies on Si-substituted Er_2Fe_{17}. *J. Magn. Magn. Mater.* **1987**, *68*, 305–308. [CrossRef]
57. Wang, J.L.; Campbell, S.J.; Tegus, O.; Marquina, C.; Ibarra, M.R. Magnetovolume effect and magnetic properties of $Dy_2Fe_{17-x}Mn_x$. *Phys. Rev. B* **2007**, *75*, 174423. [CrossRef]
58. Grandjean, F.; Isnard, O.; Long, G.J. Magnetic and Mossbauer spectral evidence for the suppression of the magnetic spin reorientation in Tm_2Fe_{17} by deuterium. *Phys. Rev. B* **2002**, *65*, 064429. [CrossRef]
59. Long, G.J.; Isnard, O.; Grandjean, F. A Mossbauer spectral study of the magnetic properties of Ho_2Fe_{17} and $Ho_2Fe_{17}D_{3.8}$. *J. Appl. Phys.* **2002**, *91*, 1423. [CrossRef]

60. Gubbens, P.C.M.; van Apeldoorn, J.H.F.; van der Kraan, A.M.; Buschow, K.H.J. Mossbauer effect investigation of Y-Fe compounds. *J. Phys. F Met. Phys.* **1974**, *4*, 921. [CrossRef]
61. Dubiel, S.M. Relationship between the magnetic hyperfine field and the magnetic moment. *J. Alloy. Comp.* **2009**, *488*, 18–22. [CrossRef]
62. Long, G.J.; Pringle, O.A.; Grandjean, F.; Buschow, K.H.J. A Mössbauer effect study of the microscopic magnetic properties of Nd_2Fe_{17} and $Nd_2Fe_{17}N_{2.6}$. *J. Appl. Phys.* **1992**, *72*, 4845. [CrossRef]
63. Halasa, N.A.; de Pasquali, G.; Drickamer, H.G. High-pressure studies on ferrites. *Phys. Rev. B* **1974**, *10*, 154. [CrossRef]
64. Drickamer, H.G.; Frank, C.W. *Electronic Transitions and the High-Pressure Chemistry and Physics of Solids*; Chapman and Hall: London, UK, 1973.